Influence of boundary stress singularities on the vibration of clamped and simply-supported sectorial plates with arbitrary radial edge conditions

O.G. McGee III [a],*, J.W. Kim [b], Y.S. Kim [c]

[a] Department of Mechanical Engineering, Howard University, Washington, DC, USA
[b] Department of Architectural Engineering, Semyung University, Jecheon, Chungbuk, South Korea
[c] Georgia Department of Transportation, Atlanta, GA, USA

ARTICLE INFO

ABSTRACT

This paper extends previous studies made for sectorial plates having re-entrant (i.e., interior) corners causing stress singularities, to provide accurate frequencies when the circular edge is either clamped or simply-supported. An extensive review of the literature is also given herein spanning nearly the past two decades explaining the free vibration characteristics of sectorial plates. In this work, the classical Ritz method is employed with two sets of admissible functions assumed for the transverse vibratory displacements. These sets include: (1) mathematically complete algebraic–trigonometric polynomials which guarantee convergence to exact frequencies as sufficient terms are retained and (2) corner functions which account for the bending moment singularities at the re-entrant vertex corner of the radial edges having arbitrary edge conditions. Extensive convergence studies summarized herein confirm that the corner functions substantially enhance the convergence and accuracy of non-dimensional frequencies for sectorial plates having either a clamped or hinged circumferential edge and various combinations of clamped, hinged, and free conditions on the radial edges. Accurate (to at least four significant figure) frequencies and normalized contours of the transverse vibratory displacement are presented for the spectra of sector angles [90°, 180° (semi-circular), 270°, 300°, 330°, 350°, 355°, 360° (complete circular)] causing a re-entrant vertex corner of the radial edges. For sector angles of 360°, a clamped–clamped, clamped–hinged, clamped–free, hinged–free or free–free radial crack ensues. One general observation is the substantial reduction in the first six frequencies as the sector angle increases for all plates, except in the first two modes of plates having free–free radial edges.

© 2010 Elsevier Ltd. All rights reserved.

1. Introduction

Documented in the literature spanning nearly two centuries are hundreds of technical publications explaining the free vibration characteristics of complete circular and annular plates with various support conditions along the circumferential boundaries or at interior points. Extensive narratives of this large body of work have been chronicled in a summarizing monograph [1] and a series of review articles [2–4]. The scope of previous work done for the sectorial plate (see Fig. 1),

---

* Corresponding author.
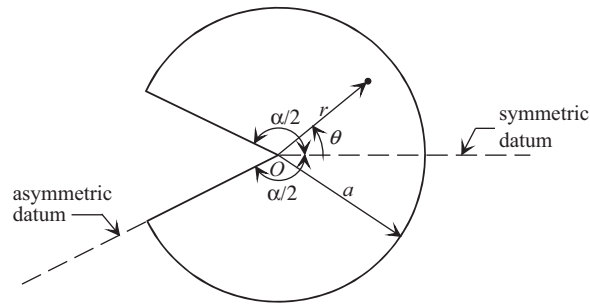 E-mail address: ogmcgee@yahoo.com (O.G. McGee III).

Fig. 1. Geometric description of a sectorial plate.

in comparison, is somewhat smaller, albeit extensive, as described in detail in the next section. Here, an extensive review of the literature covers over the past two decades of approximately a hundred publications elucidating the free vibration characteristics of sectorial plates. Several authors have offered approximate theoretical and experimental vibration data for thin sectorial and annular sector plates with various edge conditions on the circular and radial edges, namely Ben-Amoz [5], Westmann [6], Bhattacharya and Bhowmic [7], Rubin [8], Ramakrishnan and Kunukkasseril [9], Irie et al. [10], Maruyama and Ichinomiya [11], Kim and Dickinson [12], and Mizusawa [13,14]. Bapu Rao et al. [15] and Guruswamy and Yang [16] proposed various Reissner sector plate finite element formulations for approximate vibration analysis of thick circular and annular sectorial plates. Cheung and Chan [17] offered a three-dimensional curved finite strip method for static and vibration analyses of thin and thick sectorial plates with arbitrary conditions on the circular and radial edges. Srinivasan and Thiruvenkatachari [18,19] reported natural frequencies of moderately thick Mindlin and laminated composite annular sector plates with clamped circular and radial edges. Indeed, these investigations collectively provide a solid groundwork for gaining a proper perspective of the significance of the title problem in the vibration literature.

Exact solutions for frequencies and mode shapes have long been known to exist for sectorial plates having simply-supported radial edges, with arbitrary boundary conditions along the circular edge [1]. However, it has been shown [20,21] that such solutions are not applicable when the sector angle α exceeds 180° (forming a re-entrant corner, see Fig. 1). An exact solution for this situation involves non-integer order ordinary and modified Bessel functions of the first and second kinds, and particular relationships among the four constants of integration to satisfy the corner stress singularities properly. This analytical procedure has been extended to the flexural vibrations of thick sectorial plates having simply-supported radial edges forming re-entrant corners [22] using Mindlin plate theory. The Mindlin sectorial plates call for a Bessel function solution similar to that of classical thin plates, but with six, instead of four, interrelated constants of integration.

In spite of the existence of a number of semi-analytical solutions [23,14], one finds it intractable to derive exact solutions for sectorial plates with other combinations of clamped, simply-supported, and free radial edges (i.e., not both edges simply-supported). In fact, little published vibration data exists for such sectorial plates with re-entrant angles ($\alpha > 180°$) or for the special case of a semi-circular plate ($\alpha = 180°$), albeit a substantial amount of data exist for salient angles ($\alpha < 180°$) [12]. In some recent papers incorporating corner stress singularity effects [20–22,24–26], accurate (five significant figure) frequencies and mode shapes were presented for sectorial plates with free circumferential edge and clamped or free radial edges, and for completely free circular plates with rigidly constrained or free V-notches.

The present work examines sectorial plates having either a clamped or simply-supported circumferential edge, and all combinations of clamped, simply-supported, and free radial edges, including stress singularity effects at the sharp vertex corner (see Fig. 1). For a very small notch angle, 360°-α (say, one degree or less), a deep, rigidly constrained, hinged, or free radial crack ensues. A Ritz procedure is employed in which the transverse displacement field is approximated as a hybrid set of trial functions consisting of a complete set of admissible algebraic–trigonometric polynomials in conjunction with an admissible set of corner functions that exactly model the singular vibratory moments which exist at the vertices of corner angles (α) which exceed 180° [27,28]. The first set guarantees convergence to exact frequencies as sufficient terms are retained. The second set substantially accelerates the convergence of frequencies, which is demonstrated through convergence studies summarized herein. Accurate non-dimensional frequencies are presented as the sector angle α is varied. To better understand the effects of the stress singularities existing in the title problem, normalized contour plots of the vibratory transverse displacements are studied for plates having sector angles α=90°, 180° (semi-circular), 270°, 300°, 330°, 355°, and 360° (sharp radial crack).

2. Background

2.1. Recent studies of sector plate vibrations

Jomehzadeh and Saidi [29] provided recently an exact analytical solution for the free vibration of an isotropic sector Mindlin plate having simply-supported radial edges and arbitrary conditions along the circular edge. By introducing

a boundary layer function the three coupled governing equations of motion were converted into two uncoupled equations solved satisfying the boundary conditions for the natural frequencies. Non-dimensional frequency parameters were reported for a wide range of salient ($\alpha \leq 180$) and re-entrant ($180 < \alpha \leq 360$) angles, thickness–radius ratios and various boundary conditions along the circular edge.

Based on the Levinson plate theory and the first-order shear deformation plate theory, the bending analysis of functionally graded thick circular sector plates was provided by Sahraee [30]. The non-homogeneous mechanical properties of plate, graded through the thickness, were described by a power function of the thickness coordinate. Closed-form Levinson plate bending solutions of functionally graded sectorial plates were expressed in terms of the solutions of the classical plate theory for homogeneous sectorial plates and verified with previously published known solutions.

In this study, Aghdam and Mohommadi [31] bending analysis of a moderately thick orthotropic sector plate subjected to various loading conditions is presented. Different boundary conditions, including clamped, simply-supported, and free were considered. The governing equations, assuming Reissner shear deformation theory, include eight first-order partial differential equations in terms of r and θ with eight unknowns, i.e., displacements, rotations, bending and twisting moments, and shear forces within the domain. Assuming unknown variables, as separable functions of r and θ together with an extended Kantorovich method resulted to dual sets of eight first-order ordinary differential equations, which were solved iteratively. Aghdam and Mohommadi [31] showed that a Kantorovich-based approach provided accurate predictions for all displacement and stress resultant components with very fast convergence, when the accuracy of the predicted results were examined against other published data in the literature. Finite element analysis was also used to validate results for a wide range of loading and boundary conditions of sector plates.

Sharma et al. [32] presented a simple formulation for the nonlinear dynamic analysis of shear deformable laminated sector plates made up of cylindrically orthotropic layers. Transverse bending motions were approximated as in Sharma et al. [33]. Convergence of frequencies for square plates having several combinations of simply-supported, clamped, and free edge conditions was considered. Several additional effects were examined by Sharma et al. [32] including boundary conditions, moduli ratio, lamination scheme, sector angle, and annularity on the transient deflection response, comparing step, saw-tooth, and sinusoidal loadings.

An earlier study of Sharma et al. [33] proposed a simple analytical formulation for the eigenvalue problem of buckling and free vibration analysis of shear deformable laminated sector plates of cylindrically orthotropic layers. The non-axisymmetric formulation in cylindrical coordinates was idealized in polar domain by assuming two-dimensional Chebyshev polynomials for transverse bending motions, and in the time domain by adopting a Houbolt time marching scheme with a quadratic extrapolation technique. Extensive results pertaining to critical buckling loads and natural frequencies were presented. Convergence of solutions for square plates having several combinations of simply-supported, clamped, and free edge conditions was considered, and the obtained results are compared with the results of laminated square plates and isotropic sector plates available in literature. Effects of boundary conditions, number of layers, moduli ratio, rotary and in-plane inertia, plate thickness, sector angle, and annularity were also investigated.

Wang and Wang [34] offered a differential quadrature method extended to analyze the free vibration of thin sector plates with various sector angles and six combinations of boundary conditions. Numerical results compared with existing analytical and/or numerical data indicate that convergence can be achieved with increase in number of grid points and, resulting in accurate results obtained using a 9×9 differential quadrature grid or higher.

Huang and Ho [35] offered a first known analytical solution for vibrations of a polar orthotropic Mindlin sectorial plate with simply-supported radial edges. The solution was a series solution constructed using the Frobenius method and exactly satisfies not only the boundary conditions along the radial and circular edges, but also the regularity conditions at the vertex of the radial edges. The moment and shear force singularities at the vertex were exactly considered in the solution. The correctness of the proposed solution was confirmed by comparing non-dimensional frequencies of isotropic plates obtained from the present solution with published data obtained from a closed-form solution [21,22]. Huang and Ho [35] also investigated the effects of elastic and shear moduli on the vibration frequencies of the sectorial plates with free or fix boundary conditions along the circumferential edge. A study was also carried out about the influence of elastic and shear moduli on the moment and shear force singularities at the plate origin ($r=0$) for different vertex angles.

A sector Fourier p-element for free vibration analysis of sectorial membranes was presented in Houmat [36]. The element transverse displacement was described by a fixed number of linear polynomial shape functions plus a variable number of trigonometric shape functions in the radial and circumferential directions. The polynomial shape functions were used to describe the element's nodal displacements and the trigonometric shape functions was used to provide additional freedom to the edges and the interior of the element. A number of simply-supported sectorial membranes were analyzed and solutions were compared against exact solutions as well as approximate ones using conventional sector linear finite element analysis procedures. Houmat [36] recently proposed a sector Fourier p-element applied to the transverse free vibration analysis of sectorial plates. The element was formulated in terms of a fixed number of cubic polynomial shape functions plus a variable number of trigonometric hierarchical shape functions. The cubic polynomial shape functions were used to describe the element's nodal degrees of freedom and the trigonometric hierarchical shape functions were used to give additional freedom to the edges and the interior of the element. Results were obtained for a number of sectorial plates with various boundary conditions and comparisons were made with exact and 16 degrees of freedom sector finite element solutions. Primary findings revealed that the solutions converged rapidly from above relative to exact values as the number of sector Fourier p-element trigonometric terms was increased requiring relatively few terms to achieve accurate sector

plate vibration solutions. Generally speaking, the Houmat sector Fourier *p*-element [36,37] yielded greater accuracy than the conventional 16 degrees of freedom sector finite element with fewer system degrees of freedom.

Variational procedures of representing stiffened sector plates of variable radial rigidity and thickness and resting on elastic foundations were proposed in a series of papers by Molaghasemi and Harik [38–40]. Similar variational approaches of discretizing the total energy of free flexural vibration of orthotropic curved plates in polar coordinates by the method of finite differences was adopted by Singh and Dey [41]. Here, a principle of minimization of the total energy was applied in succession with respect to each discrete displacement which yielded characteristic equations for frequencies and modes of isotropic and orthotropic sector plates.

The free vibration analysis of moderately thick sector plates based on Mindlin's first-order shear deformation theory was examined in Liu and Liew [42] using the differential quadrature (DQ) method in two-dimensional polar coordinate system. Convergence and comparison studies of the first eight frequency parameters were computed for sector plates examining the effects of different boundary conditions, relative thickness ratios, and sector angles ($30° \leq \alpha \leq 360°$) on the frequency parameter solutions reported.

Liew and Yang [43] presented accurate three-dimensional elasticity solutions for free vibration of circular plates, deriving in detail the associated frequency equations using the Ritz method with a set of orthogonal polynomial series to approximate the spatial displacements of the circular plate in cylindrical polar coordinates. The perturbation of frequency responses due to the variations of boundary conditions and thickness was investigated. Frequency parameters and three-dimensional deformed mode shapes were presented and the accuracy of these results verified by appropriate convergence studies and validated against previously published solutions.

Young and Dickinson [44] employed the Ritz method to obtain a system of characteristic algebraic equations governing the free vibration of a class of thin, flat plates which involve curved boundaries defined by polynomial expressions. The class of plates is such that each plate were discretized into four $90°$ sectorial elements allowing the modeled plates to have up to four sections of outer boundary and up to four sections of inner boundary, each described by polynomials. In the absence of symmetry, or where it is not utilized, the elements were joined together through the use of very stiff translational and rotational springs which enforce the required continuity conditions. The effects of various complicating aspects, such as the presence of internal point or line supports, concentrated masses, and stepped thickness geometry, were also examined on natural frequency parameters of several plates for which comparison results were made with those existing in the published literature and the accuracy of the Young and Dickinson Ritz approach [44] was validated. Additional results were also given for several curved plates of varying complexity which were previously not treated in the open literature.

The real time technique of time-averaged holographic interferometry has been applied by Maruyama and Ichinomiya [11] to determine the natural frequencies and the corresponding mode shapes for the transverse vibrations of clamped wedge-shaped and ring-shaped sector plates. Over 200 resonant modes were obtained for wedge-shaped sector plates and over 170 for ring-shaped sector plates. The natural frequencies obtained were expressed in terms of a dimensionless frequency parameter, and graphical charts were given depicting how these frequency parameters vary as a function of the sector angle for the wedge-shaped plates and of the radii ratio for the ring-shaped sector plates, respectively. Maruyama and Ichinomiya [11] findings of free vibration characteristics for wedge-shaped plates were compared with the analytical values obtained by other authors.

The free vibration of ring-shaped polar-orthotropic sector plates was analyzed by Irie et al. [10,45] using the Ritz method incorporating a spline function as an admissible function for the deflection of the plates, and to the study of vibration problems of variously shaped anisotropic plates including these sector plates. The transverse deflection of a sector plate was approximated as a series of the products of the deflection function of a sectorial beam and that of a circular beam satisfying the boundary conditions. The deflection function of the sectorial beam was approximately expressed by a quintic spline function, which satisfies the equation of flexural vibration of the beam at each point, essentially discretizing the beam into small elements. The frequency equation of the plate was derived by the conditions for a stationary value of the Lagrangian. Irie et al. [10,45] applied their method to predict a wide spectrum of natural frequencies and mode shapes of ring-shaped polar-orthotropic sector plates with various combinations of boundary conditions.

Two and three-dimensional finite strips are developed in Cheng and Chan [46] for the analysis of thin and thick sectorial plates, both of isotropic or orthotropic material, of constant or variable thickness, and of various combinations of boundary conditions. The displacement functions for the finite strips comprised of polynomial shape functions and beam eigenfunctions. The 2-D finite strips were derived based on plate bending theory incorporating out-of-plane displacement and the slope nodal degrees of freedom. The 3-D finite strips were formulated using three-dimensional elasticity constitutive equations, and the three displacement components in a cylindrical coordinate system were chosen as the nodal degrees of freedom. Non-dimensional frequency solutions predicted by Cheng and Chan [46] involving various boundary conditions, radii and subtended angles compared favorably with those of existing solutions in the published literature.

Bucco et al. [47] combined the finite strip method with the deflection contour method in the analysis of bending and fundamental frequency prediction of thin elastic plates of arbitrary shape. Several representative plate problems of irregular boundaries were examined and favorable comparison of results was made with other known solutions.

A 24 degree of freedom sector finite element was developed for the static and dynamic analysis of thick circular plates in Guruswamy and Yang [48] based on Reissner's thick plate theory. The elements were used to analyze the natural frequencies of an annular plate with various ratios of inner to outer radius, as well as free vibrations of clamped sector plates with various thicknesses and different sectorial angles, showing findings in good agreement with an alternative solution in which thick plate theory was used.

Circular segment shaped plates were analyzed by Khurasia and Rawtani [49] using curved-sided triangular plate bending finite elements to determine their natural frequencies and mode shapes of vibration, discussing effects of variation of plate size on the vibratory characteristics. Bhattacharya et al. [50] and Bhattacharya and Bhowmic [51] considered complicating effects of large amplitudes on the free vibration of sectorial plates.

Solutions of nodal circles and natural frequencies of free vibrations for an isotropic clamped wedge-shaped plate were reported in an early paper by Rubin [8]. These findings may be used in conjunction with an available solution for the nodal radii to find all natural frequencies (including mixed modes). The Rubin solution may also be applied to a ring-shaped sector having arbitrary boundary conditions along its circular edges.

About this same time, Cheung and Kwok [52] developed a Mindlin shear deformable plate bending finite element method to analyze the free vibrations of laminated thick plates with curved boundaries for handling in polar coordinates annular as well as circular laminated anisotropic plate vibration problems. Numerical results are presented to demonstrate the influence of geometrical shape as well as that of thickness-shear deformation on the free vibrations of both homogeneous and layered plates. Comparisons between the numerical results obtained and those presented by other investigators conveyed the accuracy of the Cheung–Kwok [52] Mindlin plate finite element analysis. It was also suggested that in the limit such finite element analyses can be also used to analyze rectangular thick plate vibrations by assuming very large radii and very small subtended angle values.

The classical Rayleigh-Ritz method in conjunction with suitable coordinate transformations was suggested by Ramaiah and Vijayakumar [53] and Ramaiah [54] to be effective for accurate estimation of natural frequencies of circumferentially truncated circular sector plates with simply-supported straight edges. An extensive amount of non-dimensional frequencies were reported for all the nine combinations of clamped, simply-supported, and free boundary conditions at the circular edges and presented in the form of graphs. Works of Ramaiah and Vijayakumar [53] and Ramaiah [54] confirmed earlier observations that sector plate vibrations is analogous to those of a long rectangular strip as the width of the plate in the radial direction becomes small in the limit.

2.2. Recent sector plate vibration studies including complicating effects of stress singularities

A method was recently presented by Huang et al. [55] for accurately determining the natural frequencies of rectangular plates having V-notches along their edges. Based on the Ritz method two sets of admissible functions simultaneously were utilized including (1) algebraic polynomials from a mathematically complete set of functions and (2) corner functions addressing the boundary conditions along the edges of the notch, and describing the stress singularities at its sharp vertex exactly. The method was demonstrated for free, square plates with a single V-notch. The effects of corner functions on the convergence of solutions were shown through comprehensive convergence studies. The corner functions accelerated convergence of results significantly. Accurate numerical results for free vibration frequencies and nodal patterns were tabulated for V-notched square plates having notch angle $\alpha=5°$ or $30°$ at different locations and with various notch depths. Huang et al. [55] findings provided the first known frequency and nodal pattern results available in the published literature for rectangular plates with V-notches.

Describing the behaviors of stress singularities correctly is essential for obtaining accurate numerical solutions of complicated problems with stress singularities. Derived are asymptotic solutions for functionally graded material (FGM) thin plates in Huang and Chang [56] and FGM thick plates in Huang et al. [57] with geometrically induced stress singularities. The classical thin-plate theory was employed in Huang and Chang [56] and Lo's higher-order shear deformable plate theory was utilized in Huang et al. [57] to establish the equilibrium equations for FGM thin and thick plates. Young's modulus was assumed to vary along the thickness and Poisson's ratio was set constant. An eigenfunction expansion procedure employed to the equilibrium equations in terms of displacement components for an asymptotic analysis in the vicinity of a sharp corner. The characteristic equations for determining the stress singularity order at the corner vertex and the corresponding corner functions were explicitly given for different combinations of boundary conditions along the radial edges forming the sharp corner. The non-homogeneous elasticity properties were present only in the characteristic equations corresponding to boundary conditions involving simple supports. In addition, the effects of material non-homogeneity following a power law on the stress singularity orders were examined by showing the minimum real values of the roots of the characteristic equations varying with the material properties and vertex angle.

The stress singularities in angular corners of plates of arbitrary thickness with various boundary conditions subjected to in-plane loading were studied by Kotousov and Lew [58] within the first-order plate theory. By adapting an eigenfunction expansion approach a set of characteristic equations for determining the structure and orders of singularities of the stress resultants in the vicinity of the vertex was developed. The characteristic equations derived in this paper incorporate that obtained within the classical plane theory of elasticity (M.L. Williams' solution) and also describe the possible singular behavior of the out-of-plane shear stress resultants induced by various boundary conditions.

Using Lo's high-order shear deformable plate theory, Huang [59] applied the eigenfunction expansion approach to investigating the Williams-type stress singularities at the vertex of a wedge. The characteristic equations for determining the orders of singularities in stress resultants were separately developed for plates under extension and bending. The characteristic equations of plates under extension differ from those in generalized plane stress cases when the clamped boundary condition was imposed along one of the radial edges around the vertex. For plates under bending, the presented characteristic equations were identical to those of first-order shear deformation plate theory (FSDPT), if the clamping was not involved in boundary conditions along the radial edges of the vertex. The orders of singularities in stress resultants, which vary with the vertex angle, were plotted for various types of boundary conditions. Huang's solutions [59] were also comprehensively compared with those obtained according to other plate theories such as classical plate theory, FSDPT and Reddy's refined plate theory.

An eigenfunction expansion solution was first developed in Huang [60] to find stress singualarities for bi-material wedges by directly solving the governing equations of the Mindlin plate theory in terms of displacement components. The singularity orders of moments and shear forces at corners were determined from the corresponding asymptotic solutions having the lowest order in r and satisfying the radial boundary conditions and continuity conditions. Huang applied his solution to thoroughly examine the singularities occurring at the interface joint of bonded dissimilar isotropic plates and at the vertex of a bi-material wedge with two simply-supported radial edges. The corresponding characteristic equations for determining the singularity orders of moments and shear forces were explicitly given in Huang [60]. The singularity orders of moment were shown in graphic form as functions of the flexural rigidity ratio and corner angle, while shear force singularity orders were given as functions of the corner angle and the shear modulus ratio multiplied by the thickness ratio. The order of moment singularity obtained here for bonded dissimilar plates was also compared with that based on the classical plate theory.

Suggesting numerous areas for further studies by researchers in the literature, Leissa [61] describes three types of situations in structural analysis where singularities at points can greatly influence the global behavior of the configuration: (1) concentrated forces acting upon flat or curved membranes, (2) concentrated moments acting upon plates or shells, and (3) sharp corner singularities in plates and shells. These singularities may have strong effects upon static or dynamic deflections, free vibration frequencies, and buckling loads. Leissa [61] suggests that the concentrated forces acting upon flat or curved membranes, or concentrated moments acting upon plates and shells, are improper models, and that correct theoretical analysis indicates that they are meaningless. Examples of sharp corners discussed in Leissa [61] are (1) the re-entrant corner of a cantilever skew plate, (2) a free circular plate with a V-notch, and (3) the obtuse corners of a simply-supported parallelogram plate.

Lui and Liew [62] offered the numerical development of the differential quadrature element method (DQEM) for free vibration analysis of the shear deformable plates in polar coordinates. This is an improvement on the global differential quadrature method. The formulations of the differential quadrature element method for polar plate vibration element were derived in detail. The convergence characteristics of the differential quadrature element method for solving the free vibration of polar plates were examined by Lui and Liew [62]. The reliability and flexibility of the differential quadrature element method were illustrated by solving several selected example polar plates having discontinuities which were not solvable directly by the global differential quadrature method. The accuracy of the differential quadrature element method was evaluated and verified by comparing the present numerical results with the existing exact or approximate solutions, or the FEM solutions computed using the software package ANSYS (Version 5.3).

McGee et al. [26] offered the first known free vibration data for thin circular plates with clamped V-notches. The classical Ritz method was employed with two sets of admissible functions assumed for the transverse vibratory displacements. These sets included: (1) mathematically complete algebraic–trigonometric polynomials which guarantee convergence to exact frequencies as sufficient terms are retained and (2) corner functions which account for the bending moment singularities at the sharp corner of the V-notch. Extensive convergence studies confirmed that the corner functions substantially enhanced the convergence and accuracy of non-dimensional frequencies for circular plates with clamped notches. Numerical results were obtained for plates having their circular edges completely free. Accurate (five significant figure) frequencies were reported in McGee et al. [26] for a wide spectrum of notch angles ($0°$, $5°$, $10°$, $30°$, $60°$, and $90°$) and depths. For very small notch angles, a rigidly constrained radial crack ensues. Some general findings revealed that for the spectrum of notch angles examined, the first six frequencies increase as the notch depth increases, more so in the higher modes than the lower ones. The frequency increase with increasing notch depth was quite substantial for the semi-circular plates, and for segmented plates with sector angles less than $180°$. For a constant notch depth, it was found that there was a substantial reduction in the first six frequencies as notch angle decreases. Normalized contours of the transverse vibratory displacement were shown for plates having $90°$ and $5°$ notches of various depths ranging from deep to very shallow. The first known frequencies and mode shapes for sectorial, semi-circular, and segmented plates with clamped radial edges were also presented as special cases of the title problem.

The first known exact analytical solutions were derived in Huang et al. [22] for the free vibrations of thick (Mindlin) sectorial plates having simply-supported radial edges and arbitrary conditions along the circular edge. The general solutions to the Mindlin differential equations of motion contain non-integer order ordinary and modified Bessel functions of the first and second kinds, and six arbitrary constants of integration. By exercising a careful limiting process, three regularity conditions at the vertex of the radial edges were invoked to yield three equations of constraint among the six constants for sector angles exceeding $180°$ (re-entrant corners). Three additional linearly independent equations among

the six constants were obtained by satisfying the three boundary conditions along the circular edge. Frequency determinant equations were derived in Huang et al. [22] for Mindlin sectorial plates with circular boundaries which were clamped, simply-supported, or free. Non-dimensional frequency parameters were presented for over a wide range of salient and re-entrant sector angles ($30° \leq \alpha \leq 360°$) and thickness-to-radius ratios of 0.1, 0.2, and 0.4. Frequency results obtained for Mindlin sectorial plates were compared to those determined for classically thin sectorial plates, and the results were found to be considerably different than those derived from thin-plate theory, particularly for the fundamental frequencies of plates having sector angles slightly greater than 180° when the circular boundary is free. The frequencies for 360° sectorial plates (i.e., circular plates having a hinged crack) were compared with those for complete circular ones.

McGee et al. [25] and Leissa et al. [63] provided the earliest known free vibration data for circular plates having V-notches with bending moment singularities at its sharp corner due to the transverse vibratory motion. A theoretical analysis was undertaken using two sets of admissible displacement functions, (1) algebraic–trigonometric polynomials and (2) corner functions. These function sets were used with the Ritz method. The first set guarantees convergence to the exact frequencies as sufficient terms are taken. The second set represents the corner singularities exactly, and accelerated convergence greatly. Numerical results were given for non-dimensional frequencies of completely free circular plates having various notch angles and depths. As the notch angle becomes very small, a sharp radial crack ensues. Convergence studies demonstrated the necessity of adding corner functions to achieve accurate frequencies. Extensive, accurate (five significant figure) frequencies were presented for the spectrum of notch angles (0°, 1°, 5°, 10°, 30°, 60°, and 90°) and depths. The effect of the Poisson ratio on the frequencies in the case of shallow notches was also investigated. Sharp notches were found to reduce each of the first six frequencies from those of a complete circular plate, whereas large notch angles increased some of the frequencies. Nodal patterns were shown for plates having 5° notches. The first known frequencies for completely free sectorial, semi-circular, and segmented plates were also given as special cases.

The present work examines sectorial plates having either a clamped or simply-supported circumferential edge, and all combinations of clamped, simply-supported, and free radial edges, including stress singularity effects at the sharp vertex corner. For a very small notch angle, 360°-α (say, one degree or less), a deep, rigidly constrained, hinged, or free radial crack ensues. In a subsequent section, accurate non-dimensional frequencies are reported as the sector angle α is varied. Normalized contour plots of the vibratory transverse displacements are also studied for plates having sector angles $\alpha=90°$, 180° (semi-circular), 270°, 300°, 330°, 355°, and 360° (sharp radial crack). The Ritz method used to predict these upper bound approximate solutions on the exact ones is described in the next section wherein the transverse displacement field is approximated as a hybrid set of trial functions consisting of a complete set of admissible algebraic–trigonometric polynomials in conjunction with an admissible set of corner functions that exactly model the singular vibratory moments which exist at the vertices of corner angles (α) which exceed 180° [25–28].

3. Methodology

Consider the polar coordinates (r, θ) originating at the vertex of the sectorial plate of radius, a, shown in Fig. 1. The transverse vibratory displacement w is defined in terms of these coordinates as follows:

$$w(r,\theta,t) = W(r,\theta)\sin\omega t, \tag{1}$$

where t is time and ω is the circular frequency of vibration. The boundary conditions for the various plates studied are identified according to the lettered edges shown in Fig. 2. Displacement trial functions are assumed as the sum of two finite sets: $W=W_p+W_c$, where W_p are algebraic–trigonometric polynomials and W_c are corner functions. The admissible
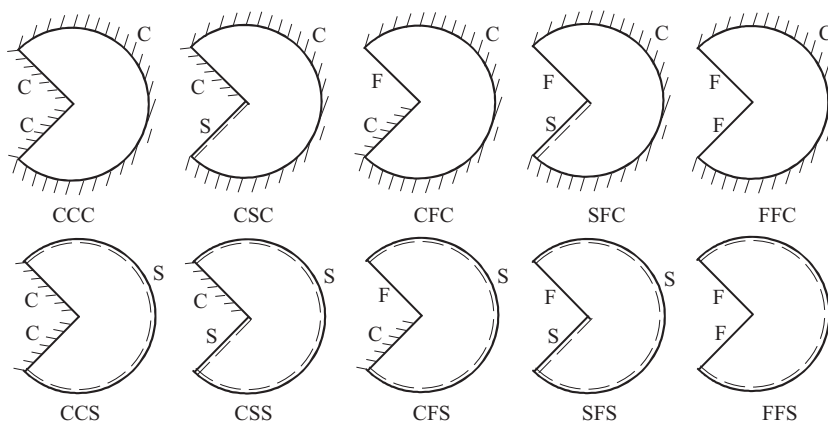

Fig. 2. Sectorial plates with various combinations of clamped, simply-supported, and free edge conditions.

polynomials for the CCC, CCS, FFC, and FFS plates are written as

$$W_p = g_1(r,\theta)\left(\sum_{m=0,2,4}^{M_1}\sum_{n=0,2,4}^{m} A_{mn}r^m\cos n\theta + \sum_{m=1,3,5}^{M_2}\sum_{n=1,3,5}^{m} A_{mn}r^m\cos n\theta\right) \tag{2}$$

for the symmetric vibration modes, and

$$W_p = g_1(r,\theta)\left(\sum_{m=2,4}^{M_3}\sum_{n=2,4}^{m} B_{mn}r^m\sin n\theta + \sum_{m=1,3,5}^{M_4}\sum_{n=1,3,5}^{m} B_{mn}r^m\sin n\theta\right) \tag{3}$$

for the anti-symmetric modes, and for the

$$\text{CCC plate}: \quad g_1(r,\theta) = (r/a)^2[(\theta/\alpha)^2 - (1/2)^2]^2(a^2 - r^2)^2, \tag{4a}$$

$$\text{CCS plate}: \quad g_1(r,\theta) = (r/a)^2[(\theta/\alpha)^2 - (1/2)^2]^2(a^2 - r^2), \tag{4b}$$

$$\text{FFC plate}: \quad g_1(r,\theta) = (a^2 - r^2)^2, \tag{4c}$$

$$\text{FFS plate}: \quad g_1(r,\theta) = (a^2 - r^2), \tag{4d}$$

each of which is defined to satisfy the essential boundary conditions along the radial edges (see Fig. 1). Also indicated in Fig. 1 are datum lines utilized to define the symmetric and anti-symmetric modes (Eqs. (2) and (3)). No symmetry exists for the CFC, CFS, SCC, SCS, SFC, and SFS plates. Thus,

$$W_p = g_2(r,\theta)\left(\sum_{m=0,2,4}^{M_1}\sum_{n=0,2,4}^{m} A_{mn}r^m\cos n\theta + \sum_{m=1,3,5}^{M_2}\sum_{n=1,3,5}^{m} A_{mn}r^m\cos n\theta + \sum_{m=2,4}^{M_3}\sum_{n=2,4}^{m} B_{mn}r^m\sin n\theta + \sum_{m=1,3,5}^{M_4}\sum_{n=1,3,5}^{m} B_{mn}r^m\sin n\theta\right), \tag{5}$$

in which for the

$$\text{CFC plate}: \quad g_2(r,\theta) = (r/a)^2(\theta/\alpha)^2(a^2 - r^2)^2, \tag{6a}$$

$$\text{CFS plate}: \quad g_2(r,\theta) = (r/a)^2(\theta/\alpha)^2(a^2 - r^2), \tag{6b}$$

$$\text{SFC plate}: \quad g_2(r,\theta) = (r/a)^2(\theta/\alpha)(a^2 - r^2)^2, \tag{6c}$$

$$\text{SFS plate}: \quad g_2(r,\theta) = (r/a)^2(\theta/\alpha)(a^2 - r^2) \tag{6d}$$

and for the CSC and CSS plates,

$$W_p = g_3(r,\theta)\left(\sum_{m=0,2,4}^{M_1}\sum_{n=0,2,4}^{m} A_{mn}r^m\cos n\theta + \sum_{m=1,3,5}^{M_2}\sum_{n=1,3,5}^{m} A_{mn}r^m\cos n\theta + \sum_{m=2,4}^{M_3}\sum_{n=2,4}^{m} B_{mn}r^m\sin n\theta + \sum_{m=1,3,5}^{M_4}\sum_{n=1,3,5}^{m} B_{mn}r^m\sin n\theta\right), \tag{7}$$

in which for the

$$\text{CSC plate}: \quad g_3(r,\theta) = (r/a)^2(\theta/\alpha)(\theta/\alpha-1)^2(a^2 - r^2)^2, \tag{8a}$$

$$\text{CSS plate}: \quad g_3(r,\theta) = (r/a)^2(\theta/\alpha)(\theta/\alpha-1)^2(a^2 - r^2). \tag{8b}$$

In Eqs. (2), (3), (5), and (7), A_{mn} and B_{mn} are arbitrary coefficients, and the values of m and n have been specially chosen to eliminate those terms which yield undesirable singularities at $r=0$, and yet, preserve the mathematical completeness of the resulting series as sufficient terms are retained. Thus, convergence to the exact frequencies is guaranteed when the series is employed in the present Ritz procedure.

The displacement polynomial Eqs. (2), (3), (5), and (7) should, in principle, yield accurate frequencies. However, the number of terms required may be computationally prohibitive. This problem is alleviated by augmentation of the displacement polynomial trial set with admissible corner functions, which introduce the proper singular vibratory moments at the vertex corner formed by the radial edges (Fig. 1). The set of corner functions is taken as

$$W_c = G(r)\sum_{k=1}^{K} C_k W_{c_k}^*, \tag{9}$$

where C_k are arbitrary coefficients, and $W_{c_k}^*$ are solutions of the fourth-order biharmonic, static equilibrium equation for bending of plates at acute corner angles [27,28]:

$$W_{c_k}^*(r,\theta) = r^{\lambda_k+1}[a_k\sin(\lambda_k+1)\theta + b_k\cos(\lambda_k+1)\theta + c_k\sin(\lambda_k-1)\theta + d_k\cos(\lambda_k-1)\theta]. \tag{10}$$

The essential boundary conditions along the radial edges $\theta = \pm\alpha/2$ may be clamped [i.e., $W(r, \pm\alpha/2) = 1/r(\partial W(r, \pm\alpha/2)/\partial\theta) = 0$], simply-supported [i.e., $W(r, \pm\alpha/2) = M_r(r, \pm\alpha/2) = 0$], or free [i.e., $V_r(r, \pm\alpha/2) = M_r(r, \pm\alpha/2) = 0$],

where M_r and V_r are the usual radial moment and shear defined elsewhere [1]. These conditions are used in Eq. (10) to construct a set of algebraic equations from which the values λ_k are obtained as roots of the vanishing determinants.

For the symmetric modes of the CCC, CCS, FFC, and FFS plates, $a_k=c_k=0$ in Eq. (10), and satisfaction of the clamped–clamped (C–C) radial edge conditions results in the following characteristic equation for the λ_k:

$$\sin\lambda_k\alpha = -\lambda_k\sin\alpha, \tag{11a}$$

whereas satisfaction of the free–free (F–F) radial edge conditions yields the alternative characteristic equation

$$\sin\lambda_k\alpha = \frac{1-v}{3+v}\lambda_k\sin\alpha. \tag{11b}$$

The corresponding corner function for the C–C edge conditions is

$$W_{c_k}^*(r,\theta) = r^{\lambda_k+1}\left[-\frac{\cos(\lambda_k-1)\alpha/2}{\cos(\lambda_k+1)\alpha/2}\cos(\lambda_k+1)\theta + \cos(\lambda_k-1)\theta\right] \tag{12a}$$

and the corner function for the F–F edge conditions is

$$W_{c_k}^*(r,\theta) = r^{\lambda_k+1}\left[\frac{\gamma_{1_k}}{\gamma_{2_k}}\frac{\sin(\lambda_k-1)\alpha/2}{\sin(\lambda_k+1)\alpha/2}\cos(\lambda_k+1)\theta + \cos(\lambda_k-1)\theta\right], \tag{12b}$$

in which

$$\gamma_{1_k} = \lambda_k(v-1)+(3+v), \quad \gamma_{2_k} = (\lambda_k+1)(v-1). \tag{12c}$$

Similarly, for the anti-symmetric modes of the CCC and CCS plates, $b_k=d_k=0$ in Eq. (10), and satisfaction of the C–C radial edge conditions results in the characteristic equation for the λ_k:

$$\sin\lambda_k\alpha = \lambda_k\sin\alpha \tag{13a}$$

and for the F–F edge conditions

$$\sin\lambda_k\alpha = -\frac{1-v}{3+v}\lambda_k\sin\alpha. \tag{13b}$$

The corner functions used for the anti-symmetric modes are analogous to those defined for the symmetric ones in Eq. (12), except the cosine functions are changed to sine functions, and vice-versa.

Satisfaction of the hinged–free (S–F) radial edge conditions results in the following characteristic equation for the λ_k,

$$\sin 2\lambda_k\alpha = \frac{v-1}{3+v}\lambda_k\sin 2\alpha. \tag{14}$$

The corresponding S–F corner function is

$$W_{c_k}^*(r,\theta) = r^{\lambda_k+1}[\sin(\lambda_k+1)\theta - \gamma_{1_k}\cos(\lambda_k+1)\theta - \gamma_{2_k}\sin(\lambda_k-1)\theta + \gamma_{3_k}\cos(\lambda_k-1)\theta], \tag{15}$$

where

$$\gamma_{1_k} = \frac{\sin(\lambda_k+1)\alpha/2}{\cos(\lambda_k+1)\alpha/2}, \tag{16a}$$

$$\gamma_{2_k} = \frac{(\lambda_k+1)(v-1)}{\lambda_k(v-1)+(3+v)}\frac{\sin(\lambda_k+1)\alpha/2}{\sin(\lambda_k-1)\alpha/2}, \tag{16b}$$

$$\gamma_{3_k} = \frac{(\lambda_k+1)(v-1)}{\lambda_k(v-1)+(3+v)}\frac{\sin(\lambda_k+1)\alpha/2}{\cos(\lambda_k-1)\alpha/2}. \tag{16c}$$

Imposition of the clamped–hinged (C–S) radial edge conditions yields the characteristic equation for the λ_k,

$$\sin 2\lambda_k\alpha = \lambda_k\sin 2\alpha \tag{17}$$

and the corresponding C–S corner function

$$W_{c_k}^*(r,\theta) = r^{\lambda_k+1}\left[\sin(\lambda_k+1)\theta - \frac{\sin(\lambda_k+1)\alpha/2}{\cos(\lambda_k+1)\alpha/2}\cos(\lambda_k+1)\theta - \frac{\sin(\lambda_k+1)\alpha/2}{\sin(\lambda_k-1)\alpha/2}\sin(\lambda_k-1)\theta + \frac{\sin(\lambda_k+1)\alpha/2}{\cos(\lambda_k-1)\alpha/2}\cos(\lambda_k-1)\theta\right]. \tag{18}$$

Finally, the characteristic equation in λ_k for the clamped–free (C–F) radial edges is

$$\sin^2\lambda_k\alpha = \frac{4}{(1-v)(3+v)} - \frac{1-v}{3+v}\lambda_k^2\sin^2\alpha \tag{19}$$

and the associated C–F corner function is

$$W_{c_k}^*(r,\theta) = r^{\lambda_k+1}[\sin(\lambda_k+1)\theta + \zeta_{1_k}\cos(\lambda_k+1)\theta + \zeta_{2_k}\sin(\lambda_k-1)\theta + \zeta_{3_k}\cos(\lambda_k-1)\theta] \tag{20}$$

with

$$\zeta_{1_k} = \frac{\mu_{1_k}}{\delta_k}, \quad \zeta_{2_k} = \frac{\mu_{2_k}}{\delta_k}, \quad \zeta_{3_k} = \frac{\mu_{3_k}}{\delta_k}, \tag{21a}$$

$$\mu_{1_k} = (\lambda_k-1)\eta_{2_k}\sin(\lambda_k+1)\frac{\alpha}{2} - (\lambda_k+1)\eta_{1_k}\cos(\lambda_k+1)\frac{\alpha}{2}\sin(\lambda_k-1)\alpha + (\lambda_k-1)\eta_{1_k}\sin(\lambda_k+1)\frac{\alpha}{2}\cos(\lambda_k-1)\alpha, \tag{21b}$$

$$\mu_{2_k} = (\lambda_k+1)\left[\eta_{1_k}\cos(\lambda_k-1)\frac{\alpha}{2} - \eta_{2_k}\cos(\lambda_k-1)\frac{\alpha}{2}\cos(\lambda_k+1)\alpha - \eta_{3_k}\sin(\lambda_k-1)\frac{\alpha}{2}\sin(\lambda_k+1)\alpha\right], \tag{21c}$$

$$\mu_{3_k} = (\lambda_k+1)\left[\eta_{1_k}\sin(\lambda_k-1)\frac{\alpha}{2} + \eta_{2_k}\sin(\lambda_k-1)\frac{\alpha}{2}\cos(\lambda_k+1)\alpha - \eta_{3_k}\cos(\lambda_k-1)\frac{\alpha}{2}\sin(\lambda_k+1)\alpha\right], \tag{21d}$$

$$\delta_k = (\lambda_k-1)\eta_{2_k}\cos(\lambda_k+1)\frac{\alpha}{2} - (\lambda_k+1)\eta_{1_k}\sin(\lambda_k+1)\frac{\alpha}{2}\sin(\lambda_k-1)\alpha - (\lambda_k-1)\eta_{1_k}\cos(\lambda_k+1)\frac{\alpha}{2}\cos(\lambda_k-1)\alpha, \tag{21e}$$

in which

$$\eta_{1_k} = \lambda_k(v-1)+(3+v), \quad \eta_{2_k} = (\lambda_k+1)(v-1), \quad \eta_{3_k} = (\lambda_k-1)(v-1). \tag{21f}$$

For the CCC, FFC, CFC, SFC, and CSC plates, the boundary function $G(r)=(a^2-r^2)^2$ in Eq. (9), whereas for the CCS, FFS, CFS, SFS, and CSS plates, $G(r)=(a^2-r^2)$. Some of the λ_k obtained from Eqs. (11), (13), (14), (17), and (19) may be complex numbers, and thus, result in complex corner functions. In such cases, both the real and imaginary parts are used as independent functions in the present Ritz procedure outlined below. Although the same analytical procedure may be followed for SSC and SSS plates [20], an exact solution has been developed for cases when the two radial edges are simply-supported [21].

In employing the Ritz method for free vibration problems, one has to construct the following frequency equations which, for the symmetric modes, are:

$$\frac{\partial}{\partial A_{mn}}(V_{\max}-T_{\max}) = 0, \quad \frac{\partial}{\partial C_k}(V_{\max}-T_{\max}) = 0 \tag{22}$$

and similarly for the anti-symmetric modes, using B_{mn} in place of A_{mn}. In Eqs. (22), the maximum strain energy, $V_{\max}$, in the plate due to bending in a vibratory cycle is

$$V_{\max} = \frac{D}{2}\iint_A [(\chi_r+\chi_\theta)^2 - 2(1-v)(\chi_r\chi_\theta-\chi_{r\theta}^2)]\,dA, \tag{23}$$

where $dA = r\,dr\,d\theta$, $D = Eh^3/12(1-v^2)$ is the flexural rigidity, h is the plate thickness, E is Young's modulus, v is Poisson's ratio, and χ_r, χ_θ, and $\chi_{r\theta}$ are the maximum bending and twisting curvatures ($\sin\omega t = 1$ assumed in Eq. (1)):

$$\chi_r = \frac{\partial^2 W}{\partial r^2}, \quad \chi_\theta = \frac{1}{r}\frac{\partial W}{\partial r} + \frac{1}{r^2}\frac{\partial^2 W}{\partial\theta^2}, \quad \chi_{r\theta} = \frac{\partial}{\partial r}\left(\frac{1}{r}\frac{\partial W}{\partial\theta}\right). \tag{24}$$

The maximum kinetic energy is

$$T_{\max} = \frac{\rho\omega^2}{2}\iint_A W^2\,dA, \tag{25}$$

where ρ is the mass per unit area of the plate. The required area integrals in the dynamical energy Eqs. (23) and (25) are performed numerically, otherwise exact integrals are tractable when λ_k is real.

Substituting Eqs. (2)–(9), (12), (15), (16), (18), (20), and (21) into (22)–(25) yields a set of homogeneous algebraic equations involving the coefficients A_{mn} (or B_{mn}) and C_k. The roots of the vanishing determinant of these equations are a set of eigenvalues, which are expressed in terms of the non-dimensional frequency parameter $\omega a^2\sqrt{\rho/D}$ commonly used in the plate vibration literature. Eigenvectors involving the coefficients A_{mn} (or B_{mn}) and C_k are determined in the usual manner by substituting the eigenvalues back into the homogeneous equations. Normalized contours of the associated mode shapes may be depicted on a $r-\theta$ grid in the sector plate domain, once the eigenvectors are substituted into Eqs. (2), (3), (5), (7), and (9).

4. Convergence studies

Having outlined the Ritz procedure employed in the present analysis, it is now appropriate to address the important question of convergence rate of frequencies, as various numbers of algebraic–trigonometric polynomials and corner functions are retained. In this section, convergence studies are summarized for sectorial plates with a 30° notch angle (i.e., $\alpha=330°$). All of the frequency and mode shape data shown in the present and following sections are for materials having a Poisson's ratio (v) equal to 0.3. Numerical calculations of all vibratory frequencies and mode shapes were performed on an IBM/RS-6000 970 power-server with an IBM/RS-6000 340 workstation cluster using double precision (14 significant figure) arithmetic.

Consider the first six non-dimensional frequencies $\omega a^2 \sqrt{\rho/D}$ for the CFC (Table 1) and SFS (Table 2) sectorial plates ($\alpha=330°$). Numerical results are shown as 40, 60, 84, and 112 polynomial terms are retained in Eqs. (2), (3), (5), or (7), in conjunction with 0, 1, 5, 10, 15, and 20 corner functions employed in Eq. (9). In these cases a larger number of polynomial terms is required due to the absence of symmetry of edge conditions.

As indicated in Table 1, the lowest frequency mode of a CFC plate exhibits a slow upper bound monotonic decrease of $\omega a^2 \sqrt{\rho/D}$ to an inaccurate value of 23.200, as the number of polynomial terms (W_p) is increased with no corner functions. That is, the polynomial series, albeit complete, is converging very slowly. An examination of the next five rows of data reveals that an accurate value to five significant figures is 20.973. Interestingly, a trial set consisting of a single corner function (corresponding to the lowest λ_k) along with a smaller number of 84 polynomial terms yields an upper bound $\omega a^2 \sqrt{\rho/D}$ value of 23.170 which is slightly lower than the 23.200 value obtained with 112 polynomial terms and no corner functions. With larger trial sets of 84 polynomials and 10 corner functions, three significant figure convergence of the lowest frequency mode is achieved. One can clearly see that by adding the first 20 corner functions to as few as 40 polynomials yields the value of 20.978, which is exact to four significant figures. For mode 2 it is seen that the addition of corner functions improves the convergence even more. Tables 1 and 2 explain similar levels of convergence accuracy in the $\omega a^2 \sqrt{\rho/D}$ values achieved by using hybrid trial sets of admissible polynomials and corner functions apropos to sectorial plates with various boundary conditions. It should be noted that the CFC (Table 1) and SFS (Table 2) cases are the two of the most challenging convergence studies (with regard to the number of corner functions required) among the ten problems analyzed here, and that the other boundary condition cases required fewer corner functions to achieve the proper convergence of frequencies.

Table 1
Convergence of frequency parameters $\omega a^2 \sqrt{\rho/D}$ for a sectorial plate having clamped–free radial edges and clamped circumferential edge ($\alpha=330°$, $v=0.3$).

Mode no.	No. of corner functions	Total number of terms in W_p			
		40	60	84	112
1	0	23.753	23.528	23.343	23.200
	1	23.475	23.321	23.170	23.046
	5	21.299	21.240	21.200	21.168
	10	20.989	20.980	20.977	20.975
	15	20.979	20.976	20.974	20.973
	20	20.978	20.975	20.974	20.973
2	0	28.773	27.884	27.190	26.700
	1	23.815	23.638	23.518	23.429
	5	22.659	22.602	22.565	22.540
	10	22.440	22.437	22.436	22.435
	15	22.438	22.436	22.435	22.435
	20	22.438	22.436	22.435	22.435
3	0	33.786	32.660	31.911	31.349
	1	33.401	32.226	31.458	30.897
	5	27.186	27.134	27.104	27.082
	10	26.992	26.988	26.985	26.983
	15	26.984	26.982	26.981	26.980
	20	26.984	26.981	26.980	26.980
4	0	41.849	40.181	39.094	38.298
	1	41.825	40.154	39.069	38.275
	5	34.672	34.581	34.513	34.465
	10	34.221	34.205	34.196	34.190
	15	34.192	34.186	34.183	34.181
	20	34.188	34.184	34.182	34.180
5	0	50.400	48.224	46.927	46.032
	1	50.277	48.066	46.790	45.918
	5	44.937	44.307	43.921	43.664
	10	42.477	42.438	42.415	42.402
	15	42.390	42.384	42.380	42.378
	20	42.382	42.380	42.378	42.377
6	0	59.704	57.256	55.836	54.882
	1	59.575	57.184	55.801	54.867
	5	57.282	55.286	54.192	53.513
	10	51.635	51.528	51.478	51.499
	15	51.454	51.428	51.415	51.407
	20	51.420	51.409	51.403	51.400

Table 2

Convergence of frequency parameters $\omega a^2 \sqrt{\rho/D}$ for a sectorial plate having simply-supported-free radial edges and simply-supported circumferential edge ($\alpha = 330°$, $v = 0.3$).

Mode no.	No. of corner functions	Total number of terms in W_p			
		40	60	84	112
1	0	13.215	13.080	12.987	12.925
	1	12.986	12.835	12.729	12.658
	5	12.504	12.482	12.467	12.459
	10	12.454	12.451	12.449	12.448
	15	12.450	12.449	12.448	12.447
	20	12.449	12.448	12.448	12.447
2	0	16.399	16.061	15.850	15.700
	1	16.029	15.758	15.581	15.453
	5	14.195	14.176	14.165	14.159
	10	14.147	14.147	14.147	14.146
	15	14.147	14.147	14.146	14.146
	20	14.147	14.147	14.146	14.146
3	0	21.290	20.503	20.007	19.664
	1	17.436	17.314	17.254	17.224
	5	17.215	17.179	17.157	17.145
	10	17.137	17.134	17.132	17.131
	15	17.133	17.132	17.131	17.131
	20	17.132	17.131	17.131	17.131
4	0	25.435	24.929	24.585	24.347
	1	24.929	24.579	24.333	24.162
	5	23.503	23.484	23.471	23.465
	10	23.466	23.462	23.459	23.458
	15	23.460	23.459	23.458	23.457
	20	23.458	23.458	23.458	23.457
5	0	35.168	33.237	32.322	31.813
	1	35.147	33.234	32.321	31.810
	5	30.804	30.715	30.666	30.640
	10	30.628	30.619	30.614	30.612
	15	30.612	30.611	30.610	30.610
	20	30.610	30.610	30.610	30.610
6	0	39.573	39.145	38.925	38.801
	1	39.554	39.133	38.921	38.800
	5	38.606	38.567	38.555	38.549
	10	38.575	38.547	38.543	38.541
	15	38.546	38.542	38.540	38.540
	20	38.542	38.540	38.540	38.540

5. Frequencies and mode shapes

Tables 3 and 4 summarize the results of extensive convergence studies of the least upper bound frequency parameters $\omega a^2 \sqrt{\rho/D}$ for the first six modes of sectorial plates with increasing sector angles $\alpha = 90°$, $180°$, $270°$, $300°$, $330°$, $350°$, $355°$, and $360°$. Listed in Table 3 are frequency parameters for sectorial plates having combinations of clamped, simply-supported, and free radial edge conditions along with a clamped circumferential edge (i.e., CCC, SCC, CFC, SFC, and FFC), whereas shown in Table 4 are frequency data for plates with the same radial edge conditions and a simply-supported circumferential edge (i.e., CCS, SCS, CFS, SFS, and FFS). Plates having both radial edges simply-supported are omitted, for accurate frequencies were presented by Huang et al. [21]. Frequency parameters corresponding to the anti-symmetric modes are indicated by a superscript asterisk (∗) as appropriate to the CCS, CCC, FFS, and FFC plates. All frequency results are guaranteed upper bounds to exact values (typically accurate to the five significant figures shown in Tables 3 and 4). Hence, Tables 3 and 4 provide an accurate database of frequencies for sectorial plates having various edge conditions and notch angles against which future results using experimental or theoretical methods (such as finite element analysis) may be compared. Frequencies of sectorial plates having free circumferential edges are available (see [21,24,26]).

A slight deterioration in the convergence of $\omega a^2 \sqrt{\rho/D}$ may occur for large $W_p + W_c$, which is attributed to the onset of matrix ill-conditioning due to round-off errors. It should be noted that the associated eigenvalue problem is positive definite, and thus, the frequency data shown in Tables 3 and 4 were obtained by using a QL algorithm combined with Cholesky factorization [64,65]. For large trial sets of polynomials and corner functions, however, the mass operator employed in the above QL algorithm may become ill-conditioned. Hence, a small amount of the data in Tables 3 and 4 were

Table 3

Frequency parameters $\omega a^2 \sqrt{\rho/D}$ for sectorial plates having arbitrary radial edge conditions and clamped circumferential edge (v=0.3).

Case	α (deg.)	Mode number					
		1	2	3	4	5	6
CCC	90	48.786	87.774[a]	104.88	136.93	164.57[a]	180.71
	180	28.125	41.726[a]	58.677	71.950	78.375[a]	94.924[a]
	270	23.743	30.041[a]	39.399	50.241[a]	62.192	64.352
	300	23.246	28.005[a]	35.967	45.278[a]	55.590	63.347
	330	22.956	26.455[a]	33.277	41.389[a]	50.383	60.147[a]
	350	22.834	25.630[a]	31.790	39.238[a]	47.506	56.473[a]
	355	22.810	25.447[a]	31.450	38.745[a]	46.848	55.634[a]
	360	22.789	25.275[a]	31.133	38.287[a]	46.269	54.897[a]
CSC	90	41.726	78.375	94.922	125.20	151.87	167.87
	180	25.271	38.269	54.821	67.367	74.000	89.655
	270	22.575	27.884	37.143	47.787	59.588	62.368
	300	22.432	26.074	33.974	43.149	53.296	62.011
	330	22.376	24.718	31.481	39.506	48.368	57.995
	350	22.358	24.025	30.100	37.487	45.644	54.494
	355	22.355	23.875	29.783	37.025	45.020	53.691
	360	22.351	23.736	29.478	36.578	44.419	52.919
CFC	90	26.476	52.109	69.078	91.503	113.00	131.60
	180	21.501	29.295	43.458	59.486	61.193	74.420
	270	21.122	23.566	30.964	40.603	51.460	59.255
	300	21.083	22.811	28.724	37.010	46.375	56.688
	330	20.973	22.435	26.980	34.180	42.377	51.400
	350	20.880	22.326	26.028	32.610	40.161	48.466
	355	20.858	22.309	25.813	32.251	39.653	47.795
	360	20.837	22.296	25.606	31.903	39.163	47.147
SFC	90	19.660	45.088	57.666	82.477	102.42	115.45
	180	19.185	26.103	40.054	56.078	56.853	69.434
	270	20.629	21.420	28.825	38.315	49.013	59.368
	300	20.002	21.475	26.724	34.992	44.241	54.366
	330	19.669	21.842	25.075	32.367	40.488	49.375
	350	19.622	22.018	24.146	30.903	38.402	46.594
	355	19.629	22.054	23.930	30.566	37.924	45.956
	360	19.646	22.112	23.726	30.241	37.461	45.341
FFC	90	7.5632	24.760[a]	31.991	56.561	67.925[a]	77.195
	180	8.6013	19.660[a]	28.857	36.329	45.088[a]	57.665[a]
	270	9.3280	18.814[a]	22.799	32.036[a]	37.029	42.016
	300	9.4879	18.847[a]	21.720	29.610[a]	36.634	39.031
	330	9.6137	18.972[a]	20.932	27.675[a]	34.638	38.378
	350	9.6806	19.096[a]	20.534	26.585[a]	33.148	38.392
	355	9.6955	19.131[a]	20.449	26.334[a]	32.795	38.406
	360	9.7094	19.167[a]	20.370	26.096[a]	32.457	38.421

[a] Anti-symmetric modes.

obtained by using an eigenvalue extraction algorithm employing two numerical techniques: (i) a householder reduction of the dynamical matrices to bi-diagonal form with matrix diagonalization achieved by using a QL procedure with shifts [64,65] and (ii) a singular value decomposition technique (cf. Press et al. [66]) using a threshold (matrix-conditioning) number of 10^{-35}. In spite of the ill-conditioning, convergence (to at least four and sometimes five significant figures) is achieved for the first six non-dimensional frequencies presented in Tables 3 and 4.

As can be expected, the frequency parameters of sectorial plates having a clamped circumferential edge are higher than those having a simply-supported circumferential edge for all combinations of radial edge conditions. Generally speaking, one can conclude from Tables 3 and 4 that for the first six modes $\omega a^2 \sqrt{\rho/D}$ decreases as the sector angle α increases. Slight exceptions to this trend is shown in the first and second modes of the SFC and SFS plates, the second and sixth modes of the FFC plate, and the second mode of the FFS plate, all of which exhibit a slight decrease, followed by a slight increase in $\omega a^2 \sqrt{\rho/D}$ with decreasing α. However, a major exception to the trend occurs for the fundamental (i.e., lowest) frequencies of the FFC and FFS plates, which increase monotonically as α increases. In these cases the sole support of the plate is along its circular boundary, and the length of this support increases as α increases, which increases the stiffness of the plate. The higher modes have radial node lines, which are equivalent to additional supports.

The frequency results for α=360° are special cases of circular plates having what is described here as a rigidly constrained, hinged, or free sharp radial crack. It is seen in Tables 3 and 4 that only a small difference in $\omega a^2 \sqrt{\rho/D}$ exists between a rigidly constrained, hinged, or free narrow V-notch (α=355°) and a sharp radial crack (α=360°).

Table 4

Frequency parameters $\omega a^2 \sqrt{\rho/D}$ for sectorial plates having arbitrary radial edge conditions and simply-supported circumferential edge ($v=0.3$).

Case	α (deg.)	Mode number					
		1	2	3	4	5	6
CCS	90	37.457	72.951[a]	88.711	118.71	144.45[a]	159.53
	180	19.504	31.431[a]	46.601	58.548	64.544[a]	79.602[a]
	270	15.777	21.252[a]	29.442	39.092[a]	49.854	51.669
	300	15.348	19.503[a]	26.436	34.672[a]	43.916	50.743
	330	15.093	18.175[a]	24.092	31.229[a]	39.247	48.046[a]
	350	14.985	17.471[a]	22.802	29.333[a]	36.679	44.733[a]
	355	14.963	17.314[a]	22.508	28.900[a]	36.093	43.977[a]
	360	14.943	17.167[a]	22.232	28.496[a]	35.558	43.348[a]
CSS	90	31.431	64.545	79.607	107.97	132.65	147.55
	180	17.164	28.481	43.247	54.386	60.675	74.758
	270	14.830	19.454	27.527	36.973	47.591	49.861
	300	14.690	17.900	24.754	32.846	41.922	49.536
	330	14.631	16.737	22.585	29.624	37.506	46.167
	350	14.610	16.140	21.389	27.847	35.077	43.011
	355	14.606	16.010	21.115	27.441	34.522	42.288
	360	14.603	15.889	20.851	27.049	33.987	41.595
CFS	90	18.049	40.965	55.916	76.896	96.430	113.46
	180	13.828	20.707	33.180	47.359	49.023	60.807
	270	13.504	15.748	22.161	30.648	40.349	47.040
	300	13.478	15.085	20.214	27.470	35.789	45.061
	330	13.402	14.733	18.703	24.982	32.224	40.293
	350	13.335	14.620	17.881	23.606	30.257	37.657
	355	13.319	14.601	17.695	23.292	29.807	37.057
	360	13.303	14.585	17.516	22.988	29.373	36.476
SFS	90	12.498	34.872	45.608	68.868	86.609	98.448
	180	11.989	18.022	30.269	44.265	45.254	56.285
	270	13.358	13.672	20.368	28.696	38.228	47.212
	300	12.758	13.840	18.555	25.763	33.954	43.035
	330	12.447	14.146	17.131	23.457	30.610	38.540
	350	12.391	14.291	16.329	22.177	28.760	36.044
	355	12.393	14.321	16.144	21.883	28.337	35.474
	360	12.405	14.373	15.968	21.600	27.928	34.924
FFS	90	2.4426	17.167[a]	23.046	45.387	54.921[a]	63.235
	180	3.5149	12.498[a]	20.593	26.707	34.871[a]	45.608[a]
	270	4.1463	11.708[a]	15.264	23.221[a]	27.380	31.993
	300	4.2826	11.723[a]	14.319	21.089[a]	27.172	29.189
	330	4.3902	11.818[a]	13.626	19.392[a]	25.512	28.500
	350	4.4481	11.916[a]	13.274	18.441[a]	24.200	28.512
	355	4.4610	11.945[a]	13.198	18.223[a]	23.888	28.525
	360	4.4735	11.974[a]	13.129	18.015[a]	23.590	28.539

[a] Anti-symmetric modes.

Shown in Figs. 3–7 are normalized displacement contours for the first three modes of sectorial plates with various boundary conditions for $\alpha=90^\circ$, 180°, 270°, 300°, 330°, 355°, and 360°. These contour plots are normalized with respect to the maximum transverse displacement component (i.e., $-1 \le W/W_{max} \le 1$, where the negative values of W/W_{max} are depicted as dashed contour lines in Figs. 3–7, and the non-dimensional frequencies shown correspond to the data listed in Tables 3 and 4). Contour lines are shown for $W/W_{max}= \pm 0.2$, ± 0.4, ± 0.6, ± 0.8, and ± 1. Nodal patterns of each mode are shown in Figs. 3–7 as darker contour lines of zero displacement ($W/W_{max}=0$) during vibratory motion.

For CCC, CCS, FFC, and FFS sectorial plates, a horizontal nodal line passes through the vertex of the notch in the anti-symmetric mode 2. Thus, the singular vibratory stresses caused by the notch effect are considerably less, and fewer corner functions are required to achieve sufficiently accurate convergence of these modes. It is seen that a sharp notch ($\alpha=355^\circ$) causes almost radial nodal lines extending from the vertex of the notch to the circumferential edge in the symmetric mode 3 of the CCC, CCS, FFC, and FFS sectorial plates. Interestingly, the radial nodal lines in the symmetric mode 3 shift slightly away from the vertex of a 90° notch ($\alpha=270^\circ$) in these cases.

The normalized displacement contours of the FFC and FFS plates are not substantially influenced by the decrease in notch angle from 90° to 5° (see Fig. 7). In contrast, the lowest frequency (i.e., fundamental) symmetric mode of the CCC and CCS plates appear to be more strongly influenced by the notch angle than the anti-symmetric mode 2 and symmetric mode 3. In the fundamental mode, the sharp curvature and distortion of the nodal lines is quite apparent due to the notch effect, more so for the CCS plate than the CCC one. Given the absence of symmetry in the CSC and CSS displacement
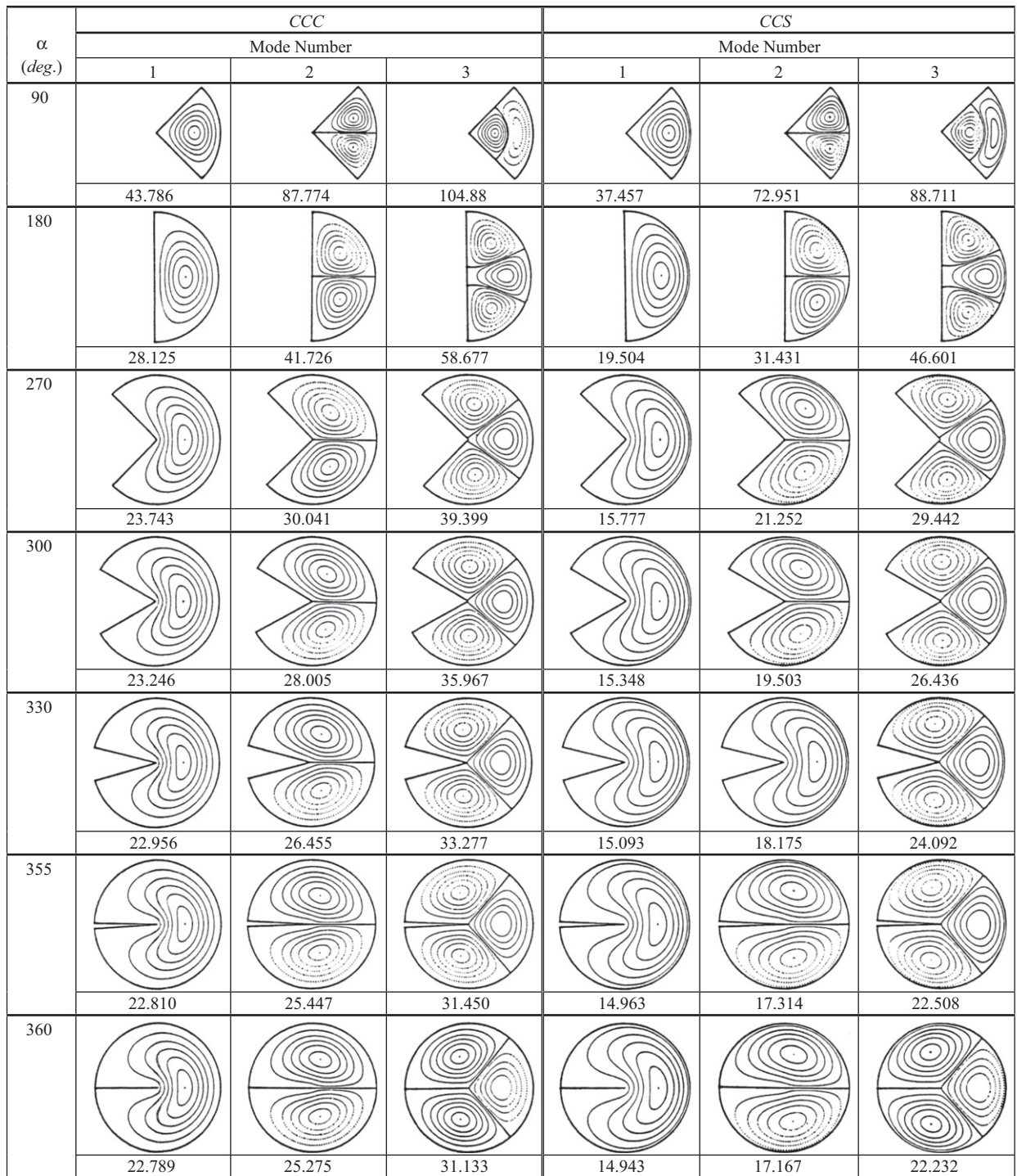
α (deg.)	CCC			CCS		
	Mode Number			Mode Number		
	1	2	3	1	2	3
90	43.786	87.774	104.88	37.457	72.951	88.711
180	28.125	41.726	58.677	19.504	31.431	46.601
270	23.743	30.041	39.399	15.777	21.252	29.442
300	23.246	28.005	35.967	15.348	19.503	26.436
330	22.956	26.455	33.277	15.093	18.175	24.092
355	22.810	25.447	31.450	14.963	17.314	22.508
360	22.789	25.275	31.133	14.943	17.167	22.232

Fig. 3. Normalized transverse displacement contours (W/W_{max}) for the first three modes of CCC and CCS sectorial plates.

contours, their nodal patterns are rotated slightly in the clockwise direction in relation to the nodal patterns of the CCC and CCS plates, respectively. As one examines the normalized displacement contours of the SFC, SFS, CFC, and CFS plates, the absence of symmetry is clear. It is interesting to note that the fundamental mode shapes for the SFC and SFS plates (Fig. 6) with $\alpha \geq 270°$ have one nodal line, which is nearly radial, whereas the second mode shapes have none. Moreover, for the 90° notch ($\alpha=270°$), the fundamental nodal patterns of the CFC and CFS plates (Figs. 3–7) are similar to those associated with mode 2 of the SFC and SFS plates (Figs. 3–7), and vice-versa. It can also be seen that mode 3 of the CFC and CFS plates

α (deg.)	CSC			CSS		
	Mode Number			Mode Number		
	1	2	3	1	2	3
90	41.726	78.375	94.922	31.431	64.545	79.607
180	25.271	38.269	54.821	17.164	28.481	43.274
270	22.575	27.884	37.143	14.830	19.454	27.527
300	22.432	26.074	33.974	14.690	17.900	24.754
330	22.376	24.718	31.481	14.631	16.737	22.585
355	22.355	23.875	29.783	14.606	16.010	21.115
360	22.351	23.736	29.478	14.603	15.889	20.815
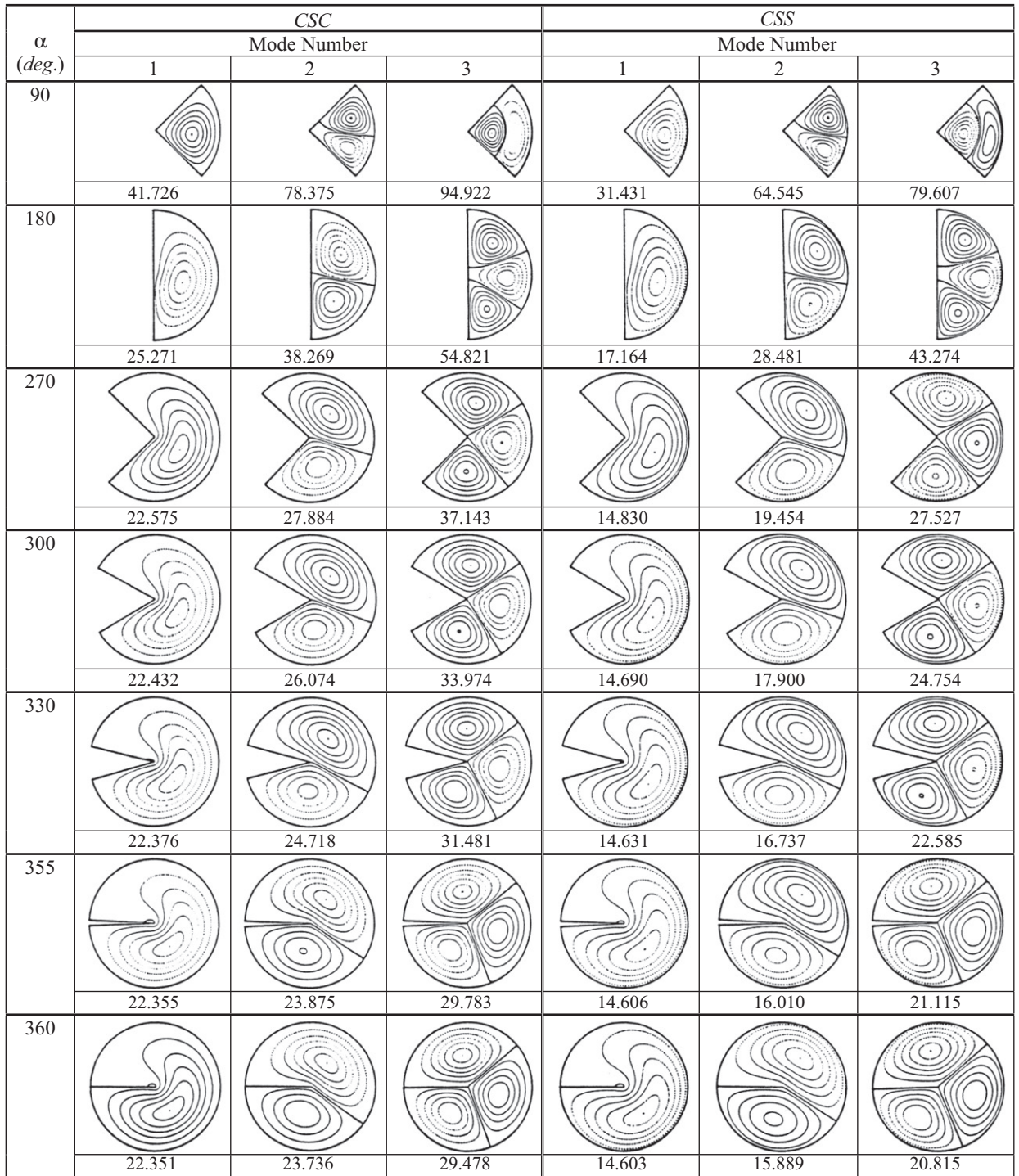
Fig. 4. Normalized transverse displacement contours (W/W_{max}) for the first three modes of CSC and CSS sectorial plates.

are analogous to mode 3 of the SFC and SFS plates, except that the horizontal radial nodal line of the former plates appears slightly rotated from the horizontal in the clockwise direction in the latter plates. Across the board in Figs. 3–7, the W/W_{max} contours and nodal patterns of the sectorial plates are only slightly changed by the clamped or simply-supported circumferential edge conditions. As expected, the contour lines $W/W_{max} = \pm 0.2$ occur closer to a simply-supported circumferential edge than a clamped one, since in the latter both the normal displacement [$W(a,\theta)$] and the bending slope [$\partial W(a,\theta)/\partial r$] vanish.
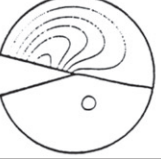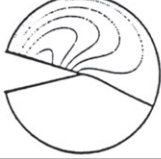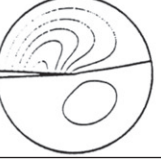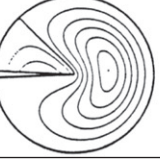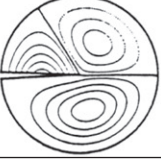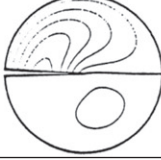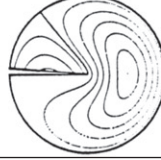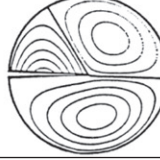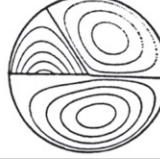
α	CFC			CFS		
	Mode Number			Mode Number		
(deg.)	1	2	3	1	2	3
90						
	26.476	52.109	69.078	18.049	40.965	55.916
180						
	21.501	29.295	43.458	13.828	20.707	33.180
270						
	21.122	23.566	30.964	13.504	15.748	22.161
300						
	21.083	22.811	28.724	13.478	15.085	20.214
330						
	20.973	22.435	26.980	13.402	14.733	18.703
355						
	20.858	22.309	25.813	13.319	14.601	17.695
360						
	20.837	22.296	25.606	13.303	14.585	17.516

Fig. 5. Normalized transverse displacement contours (W/W_{max}) for the first three modes of CFC and CFS sectorial plates.

6. Concluding remarks

Highly accurate frequencies and mode shapes for sectorial plates with a clamped or simply-supported circumferential edge and arbitrary (i.e., clamped, simply-supported, or free) radial edges have been obtained using a Ritz procedure in conjunction with classical thin-plate theory. In this approximate procedure, the assumed transverse displacement of the plate constitutes a hybrid set of complete algebraic–trigonometric polynomials along with corner functions that account

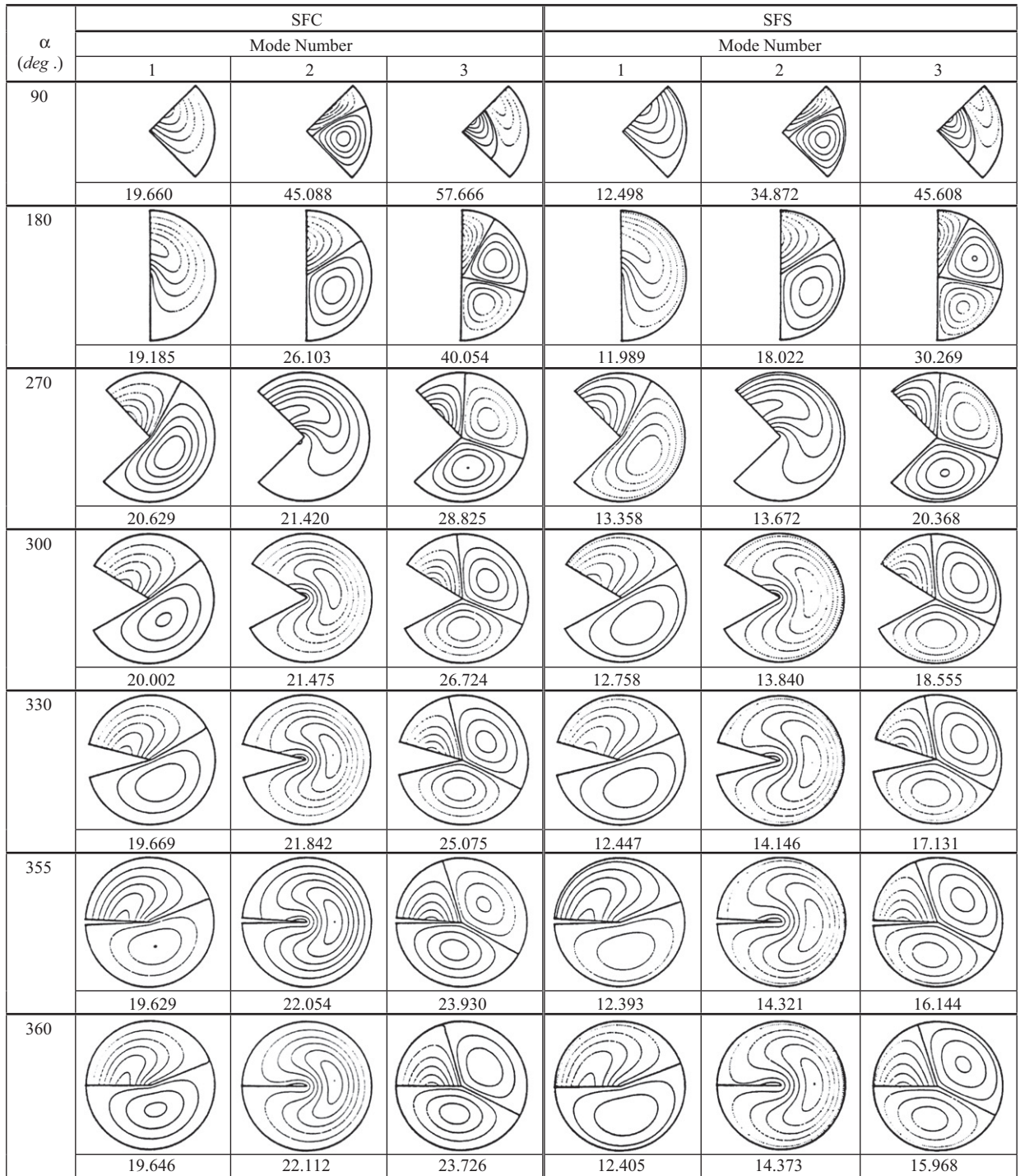| α	SFC			SFS		
(deg.)	Mode Number			Mode Number		
	1	2	3	1	2	3
90						
	19.660	45.088	57.666	12.498	34.872	45.608
180						
	19.185	26.103	40.054	11.989	18.022	30.269
270						
	20.629	21.420	28.825	13.358	13.672	20.368
300						
	20.002	21.475	26.724	12.758	13.840	18.555
330						
	19.669	21.842	25.075	12.447	14.146	17.131
355						
	19.629	22.054	23.930	12.393	14.321	16.144
360						
	19.646	22.112	23.726	12.405	14.373	15.968

Fig. 6. Normalized transverse displacement contours (W/W_{max}) for the first three modes of SFC and SFS sectorial plates.

for singular bending moments at the vertices of acute corner angles. The efficacy of such corner functions has been substantiated by an extensive convergence study of non-dimensional frequencies of clamped and simply-supported sectorial plates having all combinations of boundary conditions on the radial edges.

Detailed numerical tables have been presented, showing the variations of non-dimensional frequencies (accurate to at least four significant figures) over a wide range of vertex angles α. No results were given for the SSC or SSS cases for they exist elsewhere [20,21]. On the whole, the numerical findings reveal that the constrained radial edges, including
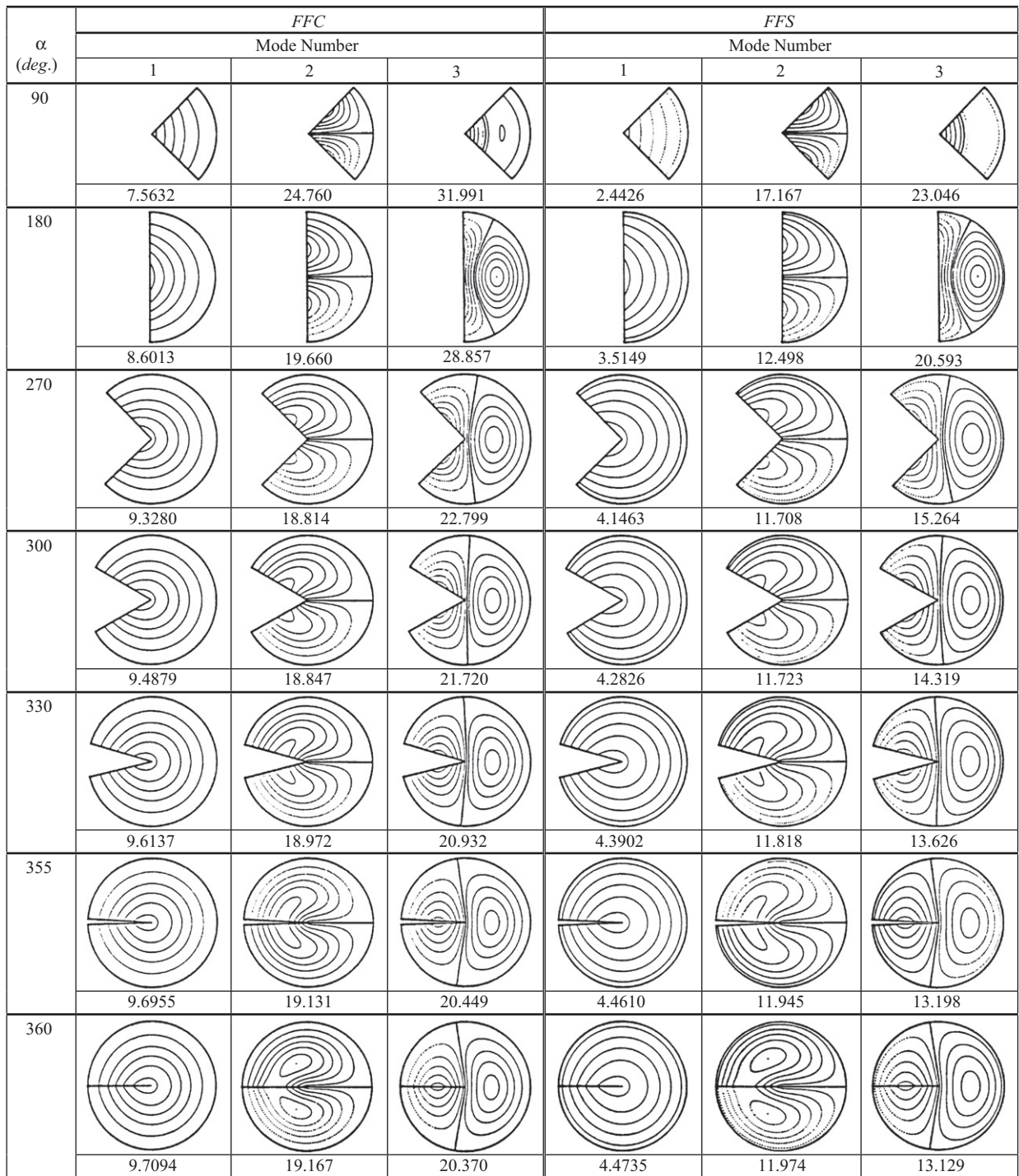
α (deg.)	FFC			FFS		
	Mode Number			Mode Number		
	1	2	3	1	2	3
90						
	7.5632	24.760	31.991	2.4426	17.167	23.046
180						
	8.6013	19.660	28.857	3.5149	12.498	20.593
270						
	9.3280	18.814	22.799	4.1463	11.708	15.264
300						
	9.4879	18.847	21.720	4.2826	11.723	14.319
330						
	9.6137	18.972	20.932	4.3902	11.818	13.626
355						
	9.6955	19.131	20.449	4.4610	11.945	13.198
360						
	9.7094	19.167	20.370	4.4735	11.974	13.129

Fig. 7. Normalized transverse displacement contours (W/W_{max}) for the first three modes of FFC and FFS sectorial plates.

singularity effects, causes the first six $\omega a^2 \sqrt{\rho/D}$ values to decrease as the sector angle α increases. This frequency decrease is observed to a larger extent in the higher modes than in the lower ones. Some exceptions to this overall trend have been discussed in the previous section.

A fundamental conclusion explicating the title problem is that the large bending moment stresses in the neighborhood of the vertices of clamped, simply-supported, or free radial edges of vibrating sectorial plates do indeed significantly influence the frequencies.

Besides this, some new understanding has been offered here about the mode shapes of sectorial plates with clamped, simply-supported, or free circumferential and radial edges. As one examines the nodal patterns and normalized transverse displacement contours of the sectorial plates presented herein, it can be seen that a deep wide notch (α=270°) or sharp crack (α=355°) causes noticeably distorted and complicated nodal lines in the first three modes. Generally speaking, for $\alpha > 180°$ highly localized bending stresses at the vertex of rigidly constrained, hinged, or free radial edges of sectorial plates may become detrimental in connection with vibration. This is because the singular stresses at the constrained vertex of sectorial plates with $\alpha \geq 355°$ can become quite serious during vibration by constituting an origin for crack propagation during fatigue. Reinforcement and repair of such crack propagation and growth with a rigid material or hinge may serve to increase the plate resistance somewhat to localized fatigue stresses during transverse vibration. Of course, it must be realized that it is not possible to produce perfectly sharp notches in plates. That is, the boundary curvature at the notch vertex will always be finite, instead of infinite. Then the vibratory bending stresses will also remain finite. Nevertheless, numerical frequencies from the present study should closely approximate those of non-sharp notches, if the notch radii are very small.

The present variational Ritz approach is computationally effective for modeling the unbounded vibratory stresses, which exist at the sharp vertex corners of constrained radial edges of sectorial plates. There is a need for future investigators to consider other types of edge conditions (e.g. edges with translational and rotational constraints). Some fundamental mechanics understanding of the effect of these localized stresses on constrained sectorial plate dynamics can be obtained through careful examination of the frequency and mode shape data reported herein. A point of methodological procedure is that investigators using continuum-based and discrete element-based formulation will have difficulty in calculating accurate solutions to the title problem unless they explicitly consider in the assumed displacement or stress fields the moment singularities at the sharp re-entrant corner ($\alpha > 180°$). Most of all, the accurate vibration data presented here serves as benchmark values for comparison with data obtained using modern experimental and alternative theoretical approaches.

Acknowledgments

References

[1] A.W. Leissa, *Vibration of Plates, NASA SP-160*, U.S. Government Printing Office, Washington, DC, 1969 (Reprinted by The Acoustical Society of America, 1993).
[2] A.W. Leissa, Recent research in plate vibrations: classical theory, *The Shock and Vibration Digest* 9 (10) (1977) 13–24.
[3] A.W. Leissa, Plate vibration research, 1976–1980: classical theory, *The Shock and Vibration Digest* 13 (9) (1981) 11–22.
[4] A.W. Leissa, Recent studies in plate vibrations: 1981–1985, part I, classical theory, *The Shock and Vibration Digest* 19 (2) (1987) 11–18.
[5] M. Ben-Amoz, Note on deflections and flexural vibrations of clamped sectorial plates, *ASME Journal of Applied Mechanics* 26 (1) (1959) 136–137.
[6] R.A. Westmann, A note on free vibrations of triangular and sector plates, *Journal of Aerospace Science* 29 (9) (1962) 1139–1140.
[7] A.P. Bhattacharya, K.N. Bhowmic, Free vibration of a sectorial plate, *Journal of Sound and Vibration* 41 (4) (1975) 503–505.
[8] C. Rubin, Nodal circles and natural frequencies for the isotropic wedge, *Journal of Sound and Vibration* 39 (4) (1975) 523–526.
[9] R. Ramakrishnan, V.X. Kunukkasseril, Free vibration of annular sector plates, *Journal of Sound and Vibration* 30 (1) (1973) 127–129.
[10] T. Irie, G. Yamada, F. Ito, Free vibration of polar-orthotropic sector plates, *Journal of Sound and Vibration* 67 (1979) 89–100.
[11] K. Maruyama, O. Ichinomiya, Experimental investigation of free vibrations of clamped sector plates, *Journal of Sound and Vibration* 74 (4) (1981) 563–573.
[12] C.S. Kim, S.M. Dickinson, On the free, transverse vibration of annular and circular, thin, sectorial plates subjected to certain complicating effects, *Journal of Sound and Vibration* 134 (1989) 407–421.
[13] T. Mizusawa, Application of the spline element method to analyze vibration of annular sector plates, *Journal of Sound and Vibration* 149 (3) (1991) 461–470.
[14] T. Mizusawa, Vibration of thick annular sector plates using semi-analytical methods, *Journal of Sound and Vibration* 150 (2) (1991) 245–259.
[15] M.N. Bapu Rao, P. Guruswamy, K.S. Sampath Kumaran, Finite element analysis of thick annular and sector plates, *International Journal of Nuclear Engineering and Design* 41 (1977) 247–255.
[16] P. Guruswamy, T.Y. Yang, A sector finite element for dynamic analysis of thick plates, *Journal of Sound and Vibration* 62 (1979) 505–516.
[17] M.S. Cheung, M.Y.T. Chan, Static and dynamic analysis of thin and thick sectorial plates by finite strip method, *Computers and Structures* 14 (1981) 79–88.
[18] R.S. Srinivasan, V. Thiruvenkatachari, Free vibration of transverse isotropic annular sector Mindlin plates, *Journal of Sound and Vibration* 101 (2) (1985) 193–201.
[19] R.S. Srinivasan, V. Thiruvenkatachari, Free vibration analysis of laminated annular sector plates, *Journal of Sound and Vibration* 109 (1986) 89–96.
[20] A.W. Leissa, O.G. McGee, C.S. Huang, Vibration of sectorial plates having corner stress singularities, *ASME Journal of Applied Mechanics* 60 (1993) 134–140.
[21] C.S. Huang, A.W. Leissa, O.G. McGee, Exact analytical solutions for the vibrations of sectorial plates with simply-supported radial edges, *ASME Journal of Applied Mechanics* 60 (1993) 478–483.
[22] C.S. Huang, O.G. McGee, A.W. Leissa, Exact analytical solutions for free vibrations of thick sectorial plates with simply-supported radial edges, *International Journal of Solids and Structures* 31 (11) (1994) 1609–1631.
[23] I.E. Harik, H.R. Molaghasemi, Analytical solution to free vibration of sector plates, *ASCE Journal of Engineering Mechanics* 115 (12) (1989) 2709–2722.
[24] A.W. Leissa, O.G. McGee, C.S. Huang, Vibrations of circular plates having V-notches or sharp radial cracks, *Journal of Sound and Vibration* 161 (2) (1993) 227–239.
[25] O.G. McGee, A.W. Leissa, C.S. Huang, Vibrations of completely free sectorial plates, *Journal of Sound and Vibration* 164 (3) (1993) 565–569.

[26] O.G. McGee, A.W. Leissa, C.S. Huang, J.W. Kim, Vibrations of circular plates with clamped V-notches or rigidly constrained radial cracks, *Journal of Sound and Vibration* 181 (2) (1995) 185–201.
[27] M.L. Williams, Surface stress singularities resulting from various boundary conditions in angular corners of plates under bending, *Proceedings of the First U.S. National Congress of Applied Mechanics* (1951) 325–329.
[28] C.S. Huang, 1991. Singularities in Plate Vibration Problems, PhD Dissertation, The Ohio State University, Columbus, OH, U.S.A.
[29] E. Jomehzadeh, A.R. Saidi, Analytical solution for free vibration of transversely isotropic sector plates using a boundary layer function, *Thin-Walled Structures* 47 (1) (2009) 82–88.
[30] S. Sahraee, Bending analysis of functionally-graded sectorial plates using Levinson plate theory, *Composite Structures* 88 (4) (2009) 548–557.
[31] M.M. Aghdam, M. Mohammadi, Bending analysis of thick orthotropic sector plates with various loading and boundary conditions, *Composite Structures* 88 (2) (2009) 212–218.
[32] A. Sharma, Y. Nath, H.B. Sharda, Nonlinear transient analysis of moderately thick laminated composite sector plates, *Communications in Nonlinear Science and Numerical Simulation* 12 (6) (2007) 1101–1114.
[33] A. Sharma, H.B. Sharda, Y. Nath, Stability and vibration of thick laminated composite sector plates, *Journal of Sound and Vibration* 287 (1–2) (2005) 1–23.
[34] X. Wang, Y. Wang, Free vibration analyses of thin sector plates by the new version of differential quadrature method, *Computer Methods in Applied Mechanics and Engineering* 193 (36–38) (2004) 3957–3971.
[35] C.S. Huang, K.H. Ho, An analytical solution for vibrations of a polarly orthotropic Mindlin sectorial plate with simply-supported radial edges, *Journal of Sound and Vibration* 273 (1-2) (2004) 277–294.
[36] A. Houmat, A sector Fourier p-element for free vibration analysis of sectorial membranes, *Computers and Structures* 79 (12) (2001) 1147–1152.
[37] A. Houmat, A sector Fourier p-element applied to free vibration analysis of sectorial plates, *Journal of Sound and Vibration* 243 (2) (2004) 269–282.
[38] H.R. Molaghasemi, I.E. Harik, Free vibration of stiffened sector plates, *Journal of Sound and Vibration* 190 (4) (1996) 726–732.
[39] H.R. Molaghasemi, I.E. Harik, Free vibration and dynamic stiffening of sector plates with radial variation in rigidity, *Journal of Sound and Vibration* 169 (2) (1994) 284–288.
[40] H.R. Molaghasemi, I.E. Harik, Natural frequencies of vibrating sector plates with stepped thickness, *Journal of Sound and Vibration* 149 (2) (1991) 323–326.
[41] J.P. Singh, S.S. Dey, Variational finite difference method for free vibration of sector plates, *Journal of Sound and Vibration* 136 (1) (1990) 91–104.
[42] F.L. Liu, K.M. Liew, Free vibration analysis of Mindlin sector plates: numerical solutions by differential quadrature method, *Computer Methods in Applied Mechanics and Engineering* 177 (1–2) (1999) 77–92.
[43] K.M. Liew, B. Yang, Three-dimensional elasticity solutions for free vibrations of circular plates: a polynomials-Ritz analysis, *Computer Methods in Applied Mechanics and Engineering* 175 (1–2) (1999) 189–201.
[44] P.G. Young, S.M. Dickinson, Further studies on the vibration of plates with curved edges, including complicating effects, *Journal of Sound and Vibration* 177 (1) (1994) 93–109.
[45] T. Irie, K. Tanaka, G. Yamada, Free vibration of a cantilever annular sector plate with curved radial edges, *Journal of Sound and Vibration* 122 (1) (1988) 69–78.
[46] M.S. Cheung, M.Y.T. Chan, Static and dynamic analysis of thin and thick sectorial plates by the finite strip method, *Computers and Structures* 14 (1-2) (1981) 79–88.
[47] D. Bucco, J. Mazumdar, G. Sved, Vibration analysis of plates of arbitrary shape—a new approach, *Journal of Sound and Vibration* 67 (2) (1979) 253–262.
[48] P. Guruswamy, T.Y. Yang, A sector finite element for dynamic analysis of thick plates, *Journal of Sound and Vibration* 62 (4) (1979) 505–516.
[49] H.B. Khurasia, S. Rawtani, Vibration analysis of circular segment shaped plates, *Journal of Sound and Vibration* 67 (3) (1979) 307–313.
[50] A.P. Bhattacharya, P.C. Upadhyaya, K.N. Bhowmic, Large amplitude vibration of sectorial plates, *Journal of Sound and Vibration* 52 (1) (1977) 137–142.
[51] A.P. Bhattacharya, K.N. Bhowmic, Free vibration of a sectorial plate, *Journal of Sound and Vibration* 41 (4) (1975) 503–505.
[52] Y.K. Cheung, W.L. Kwok, Dynamic analysis of circular and sector thick, layered plates, *Journal of Sound and Vibration* 42 (2) (1975) 147–158.
[53] G.K. Ramaiah, K. Vijayakumar, Natural frequencies of circumferentially truncated sector plates with simply-supported straight edges, *Journal of Sound and Vibration* 34 (1) (1974) 53–61.
[54] G.K. Ramaiah, Flexural vibrations of polar orthotropic sector plates with simply-supported straight edges, *Journal of Sound and Vibration* 70 (4) (1980) 589–596.
[55] C.S. Huang, A.W. Leissa, S.C. Liao, Vibration analysis of rectangular plates with edge V-notches, *International Journal of Mechanical Sciences* 50 (8) (2008) 1255–1262.
[56] C.S. Huang, M.J. Chang, Corner stress singularities in an FGM thin plate, *International Journal of Solids and Structures* 44 (9) (2007) 2802–2819.
[57] C.S. Huang, O.G. McGee III, M.J. Chang, Vibrations of cracked rectangular FGM thick plates, Composite Structures (2010), to appear.
[58] A. Kotousov, Y.T. Lew, Stress singularities resulting from various boundary conditions in angular corners of plates of arbitrary thickness in extension, *International Journal of Solids and Structures* 43 (17) (2006) 5100–5109.
[59] C.S. Huang, Corner stress singularities in a high-order plate theory, *Computers & Structures* 82 (20–21) (2004) 1657–1669.
[60] C.S. Huang, Corner singularities in bi-material Mindlin plates, *Composite Structures* 56 (3) (2002) 315–327.
[61] A.W. Leissa, Singularity considerations in membrane, plate and shell behaviors, *International Journal of Solids and Structures* 38 (19) (2001) 3341–3353.
[62] F.L. Liu, K.M. Liew, Differential quadrature element method: a new approach for free vibration analysis of polar Mindlin plates having discontinuities, *Computer Methods in Applied Mechanics and Engineering* 179 (3-4) (1999) 407–423.
[63] A.W. Leissa, O.G. McGee, C.S. Huang, Vibrations of circular plates having V-notches or sharp radial cracks, *Journal of Sound and Vibration* 161 (2) (1993) 227–239.
[64] G.W. Stewart, *Introduction to Matrix Computation*, Academic Press, 1970.
[65] J. Stoer, R. Bulirsch, *Introduction to Numerical Analysis*, Springer-Verlag, New York, 1980 Article 6.7.
[66] W.H. Press, B.P. Flannery, S.A. Teukolsky, W.T. Vetterling, *Numerical Recipes—The Art of Scientific Computing*, Cambridge University Press, 1986.